hydrology

MDPI

Article

Precipitation, Vegetation, and Groundwater Relationships in a Rangeland Ecosystem in the Chihuahuan Desert, Northern Mexico

Carlos G. Ochoa [1,*], Federico Villarreal-Guerrero [2], Jesús A. Prieto-Amparán [2], Hector R. Garduño [3], Feng Huang [4] and Carlos Ortega-Ochoa [2]

[1] Ecohydrology Lab, College of Agricultural Sciences, Oregon State University, Corvallis, OR 97331, USA
[2] Facultad de Zootecnia y Ecología, Universidad Autónoma de Chihuahua, Periférico Francisco R. Almada km 1, Chihuahua 31453, Chihuahua, Mexico
[3] Campo Experimental La Campana, Instituto Nacional de Investigaciones Forestales, Agrícolas y Pecuarias (INIFAP), km 33.3, Carretera Chihuahua-Ojinaga, Aldama 32910, Chihuahua, Mexico
[4] College of Hydrology and Water Resources, China Hohai University, Nanjing 210098, China
* Correspondence: carlos.ochoa@oregonstate.edu

Abstract: For this study, conducted in a semiarid (318 mm) rangeland setting in the Chihuahuan Desert region in northern Mexico, we evaluated the seasonal and interannual variability of precipitation, vegetation, and groundwater relations. Between 2012 and 2014, a series of soil and water conservation practices (e.g., land imprinting, contour furrows, and planting of native shrub species) were conducted in several areas within the 2500 ha study site. Since 2014, the site has been gradually instrumented to monitor several hydrologic variables, including rainfall, soil water content, and groundwater. The Normalized Difference Vegetation Index (*NDVI*) and Normalized Difference Infrared Index (*NDII*) vegetation indices were used to evaluate vegetation conditions between 2007 and 2021, before and after the treatment. Soil water content and groundwater began to be monitored in 2014 and 2016, respectively. Study results show that *NDVI* and *NDII* values were higher in the years following the treatment. A negative trend in *NDVI* values was observed in the years before restoration and reversed in the post-treatment years. The relatively low levels of soil water content obtained every year followed a seasonal response to precipitation inputs characterized by a quick rise and decline at the 0.2 m depth and a more gradual rise and decline for sensors at 0.5 m and 0.8 m depths. A positive trend in groundwater levels has been observed since the onset of monitoring in 2016, with seasonal groundwater levels rising between 0.7 m and 1.3 m for most years, except for 2020, when levels dropped 1 m. The yearly recharge of the aquifer ranged between 102 mm and 197 mm. The conservation practices employed have positively affected the state of the rangeland ecosystem. The upward trends in *NDVI*, *NDII*, and groundwater levels observed in the post-treatment years were partly attributed to improved land conditions. The findings of this study contribute to the improved understanding of land use and environmental relations in summer precipitation-dominated rangeland ecosystems.

Keywords: soil moisture; arid and semiarid; groundwater; Chihuahuan Desert; rangelands; *NDVI*; *NDII*

check for updates

Citation: Ochoa, C.G.; Villarreal-Guerrero, F.; Prieto-Amparán, J.A.; Garduño, H.R.; Huang, F.; Ortega-Ochoa, C. Precipitation, Vegetation, and Groundwater Relationships in a Rangeland Ecosystem in the Chihuahuan Desert, Northern Mexico. *Hydrology* **2023**, *10*, 41. https://doi.org/10.3390/hydrology10020041

Academic Editor: Patrizia Piro

Received: 1 January 2023
Revised: 25 January 2023
Accepted: 28 January 2023
Published: 1 February 2023

1. Introduction

Many regions worldwide face long-term deficits in water available for human and environmental uses [1]. Water scarcity, particularly in arid and semiarid systems, is projected to increase due to the combined effect of climate change and a growing population [2–4], leading to greater difficulties in regions already experiencing water stress. Negative impacts caused by anthropogenic activities or natural causes in arid and semiarid landscapes include the loss of soil, degraded habitat, and decreased groundwater replenishment [5,6].

The Chihuahuan Desert ecoregion, from central Mexico to the southwestern United States, is facing severe drought conditions and excessive groundwater withdrawals to satisfy the needs of a growing population, as well as land use conversion from natural ecosystems to irrigated landscapes. Climate change projections for the region include more frequent and prolonged droughts, a shift in precipitation seasonality, and increased temperatures [7] that would result in greater evaporative losses and reduced aquifer recharge.

Land surface observation via the Landsat sensor has proven its value in monitoring ecosystems, mainly due to its long history (50 years) in terms of radiometric, spatial, temporal, and spectral resolutions, which distinguishes it from other satellite missions [8]. The sensor is increasingly used to assess the behavior of groundwater concerning precipitation, agricultural disturbances, and land cover changes, among others [9]. Of the spectral indices derived from remote sensing, which can identify areas of vegetation and its condition, the Normalized Difference Vegetation Index (*NDVI*) and Normalized Difference Infrared Index (*NDII*), among others, are used [10–12]. The *NDVI* is based on the differences in reflectance of the red spectrum regions (absorption of pigments) and the near-infrared regions (caused by cell structure). The *NDVI* is one of the most widely used spectral indices in remote sensing and a valuable tool for linking climatic variables and vegetation conditions at spatial and temporal scales [13]. The *NDVI*'s response to climatic variables has been well documented [14–16] with the *NDVI* shown to be a good predictor of groundwater [17,18]. The *NDII* was developed by Hardisky et al. [19] by implementing the relationship between the near-infrared and shortwave near-infrared regions of the spectrum. The *NDII* has been used to detect water stress in the root zone of plants [20] because the *NDII* values are sensitive to changes in the water status of the vegetation [21]. Due to this sensitivity to plant water content, the *NDII* provides more detailed information on vegetation condition than the *NDVI*. The *NDII* has shown a good relationship with root-zone soil moisture on a regional scale [22].

Groundwater is a vital resource in arid and semiarid regions [23]. The interaction of groundwater and vegetation cover in shrublands, grasslands, and riparian zones, among others, requires a better understanding of how anthropogenic impacts affect temporal variability in groundwater recharge [9]. Vegetation is a good indicator of water availability in arid environments, where groundwater behavior is mainly driven by rainfall [24], and in areas where seasonal precipitation percolating below the plants' root zone contributes to replenishment of the shallow aquifer [25,26]. Among the various techniques available to estimate groundwater recharge, the water table fluctuation method (WTFM) [27,28] has been used in multiple studies (for examples, see [26,29,30]) due to its simplicity and potential applicability in data-limited environments. The WTFM uses groundwater level data, which in some instances is readily available or can be measured directly, and the aquifer's specific yield (*Sy*) property. The WTFM assumes that rises in groundwater levels are caused by water percolating into the water table [31]. Also, it posits that *Sy* is constant over time and space. The WTFM's drawback is the difficulty in obtaining an accurate *Sy* value for a particular aquifer; these values may vary by depth, as well as over time [32,33] and space.

Soil and water conservation techniques can help restore landscapes and strengthen their resistance to change [34]. The individual or combined use of restoration methods (e.g., contour furrows, pitting, stone bunds, and plantings) common in dryland ecosystems can reduce soil erosion, improve vegetation cover and infiltration, and help with surface water retention and aquifer recharge. Techniques such as the use of stone bunds led to a 68% soil loss reduction in a study site in northern Ethiopia [35] and increased pine survival (80%) in upslope forested areas in Durango, Mexico [36]. The effect of soil conservation practices increased groundwater by 19% in the steep highlands of Ethiopia [37]. Water harvesting techniques using soil retention structures in arid and semiarid zones have improved surface water and vegetation health [38,39]. Using contour furrows and pitting techniques on desert rangelands has increased soil moisture content, plant cover, and forage production [40].

Studies on groundwater availability and vegetation conditions are limited in the semiarid rangeland settings of northern Mexico. This research examined the relationships of precipitation, soil water, vegetation, and aquifer recharge in a restored rangeland ecosystem of an endorheic basin in Chihuahua, Mexico. The study objectives were to (1) characterize precipitation, soil water, and groundwater relations following restoration and (2) assess the suitability of the *NDVI* and *NDII* indices to capture the vegetation interannual variability before and after soil and water conservation practices were established.

2. Materials and Methods

2.1. Site Description

This study was conducted in a rangeland ecosystem in the north-central region of the state of Chihuahua, Mexico (Figure 1a,b). The study site is within the Chihuahuan Desert ecoregion, where precipitation—mostly rain—ranges from 150 to 500 mm and occurs during the summer and fall [41]. The long-term (1981–2022) mean annual precipitation for the region is 318 mm. The mean annual temperature ranges from 5.0 to 31.4 °C, with the highest daily maximum temperature of 42.6 °C in June and the lowest daily minimum temperature of −12.9 °C in February (Table 1).

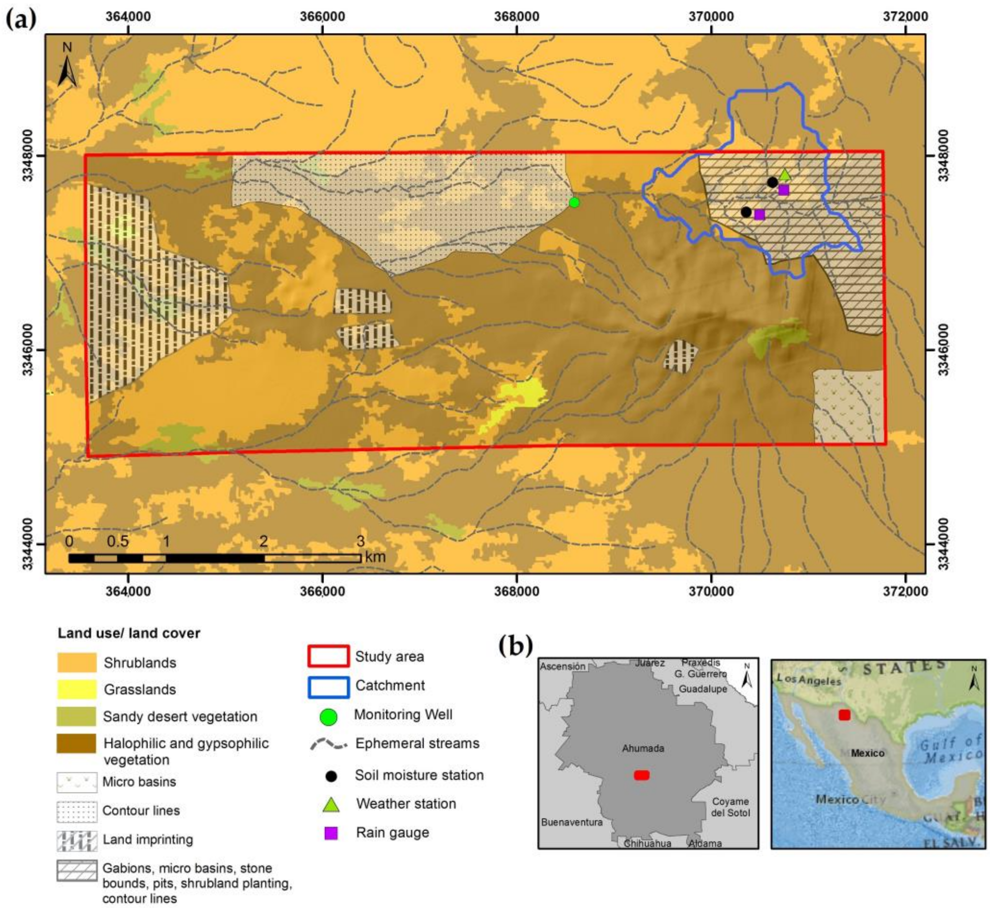

Figure 1. Location and instrumentation of the study site. (**a**) Study area showing ephemeral streams, catchment, and land cover, (**b**) Location of the study area within the municipality of Ahumada (left) and the country of Mexico (right). This map was created using ArcGIS 10.5® software. ArcGIS® is the intellectual property of ESRI and is used herein under license. Copyright © ESRI. All rights reserved. For more information about ESRI® software, please visit www.esri.com (accessed on 10 September 2022). Basemap credits: ESRI, DigitalGlobe, GeoEye, i-cubed, USDA FSA, USGS, AEX, Getmapping, Aerogrid, IGN, IGP, swisstopo, and the GIS User Community.

Table 1. Average monthly total precipitation (mm), daily maximum temperature (°C), and daily minimum temperature (°C) for 1 January 2007 to 24 December 2022 near the city of Ahumada, Chihuahua, Mexico. (Source: https://power.larc.nasa.gov/data-access-viewer/; accessed on 10 December 2022)

Month	Precipitation	Daily Maximum Temperature	Daily Minimum Temperature
January	13.3	22.7	−4.8
February	10.8	25.4	−3.9
March	9.6	29.1	−1.5
April	9.9	32.3	2.9
May	12.2	36.5	8.1
June	26.5	39.4	15.0
July	62.6	38.4	18.0
August	70.5	36.6	16.9
September	49.6	34.8	12.1
October	24.7	31.8	4.4
November	11.4	26.8	−2.1
December	16.8	23.0	−5.0

The study was conducted in the environmental management unit (EMU) "El Roble" SEDUE-EX3489/CHIH-07, encompassing an area of 2500 hectares (ha). The EMU is located between UTM coordinates 363,667.09° E, 3,347,954.14° N, and 371,658.91° E, 3,345,160.70° N (Figure 1a), at an elevation ranging from 1404 to 1766 m above sea level (masl). Vegetation at the study site comprises shrublands, grasslands, and sandy desert, as well as gypsophilic and halophilic vegetation. Besides cattle, these rangelands host numerous wildlife species typical of northern Chihuahua, including pronghorn (*Antilocapra americana)*, javelina or collared peccary (*Pecari tajacu* (*Linnaeus*, 1758)), and avian species such as aplomado falcon (*Falco femoralis*) and ferruginous hawk (*Buteo regalis*) [42]. Between 2012 and 2014, a series of soil and water conservation practices aiming to improve habitats and increase forage production were conducted in several areas within the study site. The treated area encompassed a total of 827 ha. The restoration practices included land imprinting, contour furrows, stone bunds, gabions, and planting of native shrub species (i.e., *Atriplex canescens* and *Prosopis glandulosa*) (Appendix A, Figure A1).

Soil water, groundwater, and weather data collection began in 2014 to investigate the hydrology of a catchment in the northeastern corner of the study site. Multiple ephemeral streams that flow in response to sporadic convective storms during the summer and fall are part of the landscape. The study site's soil is classified as Regosols [43], made up of deep, well-drained, medium-textured colluvium deposits.

A vegetation survey conducted in 2017 as part of this study showed that the dominant overstory vegetation is creosote bush (*Larrea tridentata)*, followed by honey mesquite (*Prosopis glandulosa*) and then whitethorn acacia (*Acacia constricta)*. The dominant understory vegetation is black grama (*Bouteloua eriopoda*), followed by tobosa (*Hilaria mutica*) and blue grama (*Bouteloua gracilis*). Herbaceous production data collected at the end of the growing season in the fall of 2013 and 2014 showed mean yield values of 630 and 536 kg ha^{-1} in treated vs. untreated areas in 2013 and 1910 and 1600 kg ha^{-1} in 2014. In addition to the physical soil and water conservation infrastructure and planting of native species, the grazing management plan was adjusted. The cattle were removed from the property during the treatment years and reintroduced in 2016 using a rotational grazing system with light to medium stocking rates.

The study site overlies a shallow aquifer system near the eastern boundary of the regional Flores Magón-Villa Ahumada aquifer. The regional aquifer is located in the closed basin system of Cuencas Cerradas del Norte, in the hydrologic region 34 in northern Mexico [44]. As described in a report by the National Water Commission of Mexico (CONAGUA) [45], the Flores Magón-Villa Ahumada aquifer sits in an alluvial and conglomeratic sedimentary deposit of medium permeability interbedded with basaltic volcanic rocks. The higher elevation parts of the basin serve as areas of recharge. It is estimated that 98.6% of water extraction in the region is used for irrigation, with the remaining 1.4% utilized for household and livestock purposes. Depth to groundwater in the regional aquifer ranged from 10 to 90 m in 2005 and from 10 to 100 m in 2010. Large cones of depression noted in 2010 resulted in a water table decline of 0.5 to 1 m for most of the aquifer and up to 4 m in some areas [45]. Water table elevations in the aquifer range from 1190 to 1470 masl. The static water table elevation in the shallow (<30 m) monitoring well at our study site, measured at baseflow conditions in the spring of 2016, was 1457 masl. The well is located near the outlet of the catchment (see Figure 1a) and provides water for livestock and household purposes as part of the ranching operation. The well has a relatively low flow (20 L min^{-1}) solar pump that runs only during the day.

2.2. Soil Water and Precipitation Data

Two soil water content stations (North and South) were installed in 2014. Each station included two vertical networks of five soil volumetric water content (θ) sensors (Model EC-5, Meter Group; Pullman, WA, USA) installed 5 m apart. The sensors were installed at 0.2, 0.5, and 0.8 m depths in one of the vertical networks and at 0.2 and 0.5 m in the other. The sensors were connected to EM-50 dataloggers (Meter Group; Pullman, WA, USA) and were programmed to record θ data hourly. The soil water sensors were not calibrated for site-specific soil properties. Soil samples collected in 2021 in the upper 0.2 m soil profile showed soil texture as sandy loam for the North station and loam for the South station. A Kruskal–Wallis One Way Analysis of Variance (ANOVA) on ranks test was conducted to evaluate daily-average θ variability by soil depth, by season (dry vs. wet), for each soil moisture station. The wet season was defined based on the months with higher precipitation levels (June to October), with the dry season therefore comprising November to May.

Precipitation on site was measured starting in March 2017. A tipping bucket rain gauge (Model HOBO RG3, Onset Computer, Corp.; Bourne, MA, USA) was installed at both the North and South stations. Precipitation was recorded hourly. A weather station (Campbell Scientific Inc.; Logan, UT, USA) equipped to measure incoming solar radiation, air temperature, relative humidity, wind speed, and wind direction was installed at the North station in November 2021 (see Figure 1a).

2.3. Groundwater Data and Aquifer Recharge

Groundwater level data was collected hourly beginning in April 2016 using a water level logger (Model HOBO U20-001-01) installed at a depth of 23.35 m in the well near the catchment's outlet (see Figure 1). The water level logger was replaced in 2018 with a newer model (MX 2001, Onset Computer, Corp.; Bourne, MA, USA) that was set to record data every two hours and allowed for data collection using Bluetooth® technology. A portable water level meter (Model dipper-T 1100, Heron Instruments, Inc.; Dundas, ON, Canada) was used to collect depth to groundwater data to verify or calibrate the water level logger data. The automated water level logger began malfunctioning early in the year and was decommissioned in fall 2021. After that, the portable water level meter was used to take depth-to-water table measurements when visits to the study site occurred.

Seasonal groundwater level fluctuations were characterized based on data collected from the monitoring well. Aquifer recharge was estimated based on groundwater level data and the WTFM using the following equation:

$$Re = \Delta h \times Sy \tag{1}$$

where Re = aquifer recharge (mm), Δh = change in water level (mm), and Sy = specific yield of the unconfined aquifer. The groundwater level sensor's data showed that the aquifer had a relatively rapid recovery rate (i.e., 2 to 3 h) after the well's solar pump was shut off during the evenings or at other times when needed (e.g., for repairs). Yet, to reduce the potential effect of groundwater pumping on aquifer recharge estimates, the maximum groundwater level values of the hourly or bi-hourly data collected daily were used in the analysis.

Based on pumping tests conducted in 2010, CONAGUA [45] reported *Sy* values ranging between 0.11 and 0.22, with an average of 0.15, for the regional Flores Magón-Villa Ahumada aquifer, where our well is located. They also reported that the *Sy* values obtained are similar to those of neighboring regional aquifers. We used the average *Sy* value of 0.15 in our *Re* calculations.

2.4. Vegetation Indices

Several studies have shown that remote sensing-based indices such as the *NDVI* can help to link vegetation and environmental changes [46,47]. We used *NDVI* and *NDII* data from the Landsat sensor to assess changes in vegetation before and after the soil and water conservation practices occurred at our study site. The pre-treatment conditions were established as those from 2007 to 2012. Most restoration practices occurred in 2012 and 2013; therefore, we defined the post-treatment years as 2014 to 2021. No 2022 *NDVI* or *NDII* data were available for comparison against other variables (i.e., groundwater and soil water content).

The *NDVI* is an indicator of the vegetation's state of health [48,49]. It is a combination of the centered, visible red (*Red*) and near-infrared (*NIR*) bands and indicates the general greenness of vegetation or photosynthetically active vegetation (Equation (2); [50,51]). The *NDII* is an indicator of the availability of humidity in the root zone of the plants [52,53]. It combines the *NIR* and shortwave infrared (*SWIR*) bands (Equation (3)). The images of the *Red*, *NIR*, and *SWIR* bands have a spatial resolution of 30 m

$$NDVI = \frac{NIR - Red}{NIR + Red} \tag{2}$$

$$NDII = \frac{NIR - SWIR}{NIR + SWIR} \tag{3}$$

where *Red*, *NIR*, and *SWIR* are the reflectance values of spectral bands in the red, near-infrared, and shortwave infrared regions, respectively. *NDVI* values range from −1 to 1. Higher *NDVI* values imply more vegetation greenness [46]. *NDII* values vary between −1 and 1. A low *NDII* value, particularly below zero, indicates water stress [54].

The Landsat sensor offers medium resolution data, counting on the oldest historical reservoir of Earth observation, from 1972 to the present. Data from the Landsat Thematic Mapper 5 (TM5) sensor, Landsat Enhanced Thematic Mapper Plus 7 (ETM + 7) sensor, and Landsat Operational Land Imager 8 (OLI8) [55,56] are adequate for time series analysis [57]. Surface reflectance data from the Landsat TM5, ETM + 7, and OLI8 were obtained using the Google Earth Engine platform (GEE, http://earthengine.google.com/, accessed on 18 September 2022; [58]) where the spectral index two was generated from the surface reflectance. We used imagery from 2007 to 2021, with a spatial resolution of 30 m and a temporal resolution of 16 days. The study area included 34,452 pixels with 108 rows and 319 columns. Images were selected based on the absence of clouds in the study area.

The relationships between vegetation and other environmental variables over time were evaluated using monthly-average *NDVI* and *NDII* data, which were compared against precipitation (*P*), air temperature (*T*), depth to groundwater (*G*), and θ. To assess the inter-annual variability of vegetation with *NDVI* and *NDII*, we selected imagery collected from August to October in each year. As described in Ni [59], the highest biomass production peak is typically exhibited in these three months. To reduce potential errors in vegetation index estimates attributed to spatial heterogeneity, we divided the area into three distinct zones (high, mid, and low elevation) based on the altitudinal gradient observed at the study site (Figure 2). The high elevation zone ranged from 1485 to 1546 masl, the mid-elevation from 1437 to 1485 masl, and the low elevation from 1404 to 1436 masl. The three elevation zones were determined using the natural breaks classification method [60] for the digital elevation model.

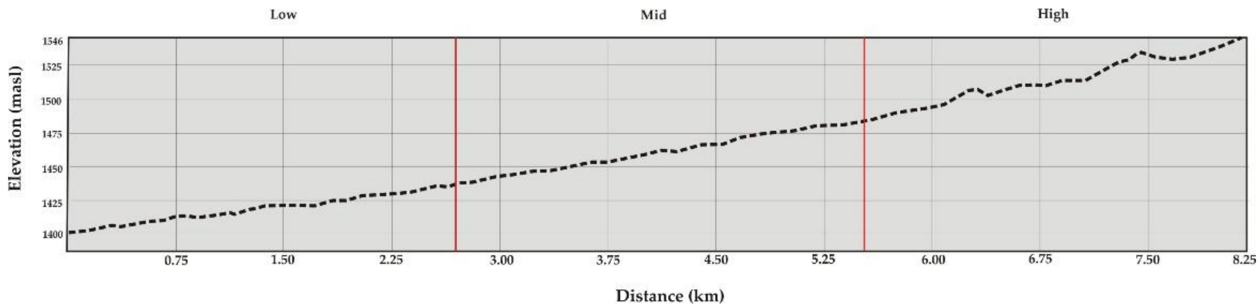

Figure 2. Profile of the study site illustrating the gradient from high (east) to low (west) elevation in meters above sea level (masl).

The Minitab 19 program (Minitab, LLC; State College, PA, USA) was used to conduct a single-factor ANOVA test for repeated samples with the *altitudinal gradient* and *time* as variables, using the hypotheses $\mu_{low} = \mu_{medium} = \mu_{high}$ and $\mu_{2007} = \ldots = \mu_{2021}$, respectively, followed by a Tukey significance test, to detect significant differences between the levels. Values of $p \leq 0.05$ were considered statistically significant.

2.5. Trend Analysis of Groundwater, Climate Variables, and Vegetation Indices

Records of P and T for 2007 to 2022 used in the trend analysis were obtained online using the POWER Data Access Viewer (https://power.larc.nasa.gov/data-access-viewer/; accessed on 10 December 2022). These data, along with *NDVI* and *NDII* data from 2007 to 2021, were used to evaluate weather (i.e., P and T) and vegetation (i.e., *NDVI* and *NDII*) trends before conservation practices occurred, as well as climate, vegetation, soil moisture, and groundwater relationships after that. The pre-treatment (2007–2012) and post-treatment (2014–2021) trends of P, T, *NDVI*, and *NDII* were determined using the trend-free prewhitened Mann-Kendall (*tfpwmk*) and Sen's slope (*sens.slope*) functions in R-Studio (Version 1.1.383—© 2009–2017 RStudio, Inc., Boston, MA, USA). The trends of G (2016–2022) and θ (2014–2022) were also evaluated using the same approach. The trend-free prewhitened Mann-Kendall test helps remove issues related to autocorrelation if the time series is not random. Sen's slope provides a value of the increase or decrease of the time series trend. In addition, the non-parametric Spearman Rank Order Correlation was used to evaluate the relationships between G and the following variables: *NDVI*, *NDII*, θ, and P. SigmaPlot® version 14.0 (Systat Software, Inc.; San Jose, CA, USA) was used in this statistical analysis.

3. Results

3.1. Soil Water

The variability of θ levels followed a seasonal trend characterized by a quick rise and decline at the 0.2 m depth and a more gradual rise and decline in θ for the sensors at 0.5 and 0.8 m depths. Figure 3 shows the average θ conditions from both stations at the various sensor depths for the entire study period. The highest θ values for all sensor depths were obtained in October 2019 and August 2021. Frequent and relatively high amounts of precipitation were observed in the summers of 2018 and 2019 [61].

The North station θ levels ranged from 0.052 to 0.214 for the 0.2 m sensor depth, from 0.029 to 0.189 for the 0.5 m depth, and from 0.076 to 0.125 for the deeper 0.8 m sensor depth. The South station θ levels ranged from 0.026 to 0.296, from 0.051 to 0.272, and from 0.051 to 0.242 for the 0.2, 0.5, and 0.8 m depths, respectively.

A closer look at the relationships between P and θ can be observed in Figure 4, which depicts daily P and θ level variability spanning three summer seasons (2015 to 2017) for the North soil water station. A sharp rise and decline in θ can be observed for the sensor at the 0.2 m depth. A less pronounced, steadier rise that generally peaked between July and August for the 0.5 m sensor and between September and October for the 0.8 m sensor was noted for most years. A storm event in October 2016 resulted in a significant rise in θ levels for the 0.5 m sensor. The higher θ levels observed at 0.8 m than at 0.5 m were attributed to finer-textured soil, which consequently increased water holding capacity, noted at that depth during sensor installation.

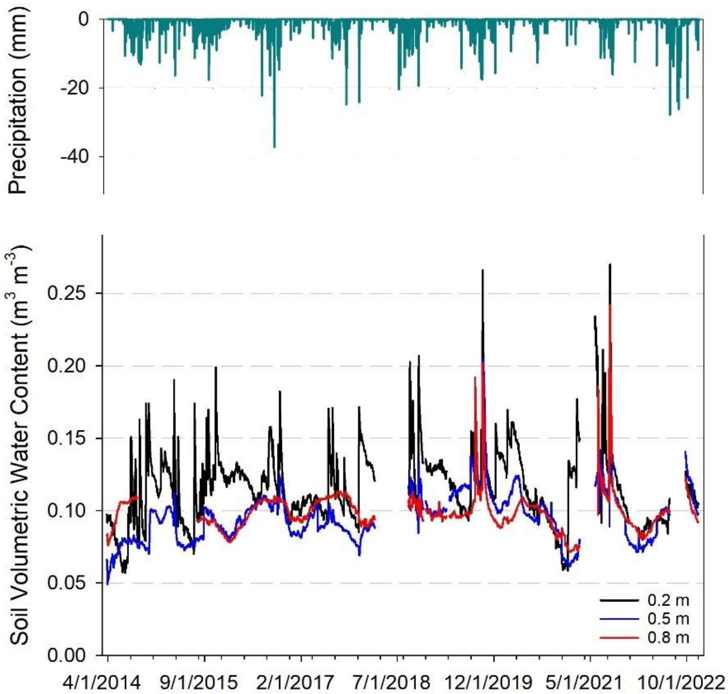

Figure 3. Daily precipitation and daily-average soil volumetric water content (θ) for all sensors at each of 0.2, 0.5, and 0.8 m depths from 26 March 2014 to 2 December 2022.

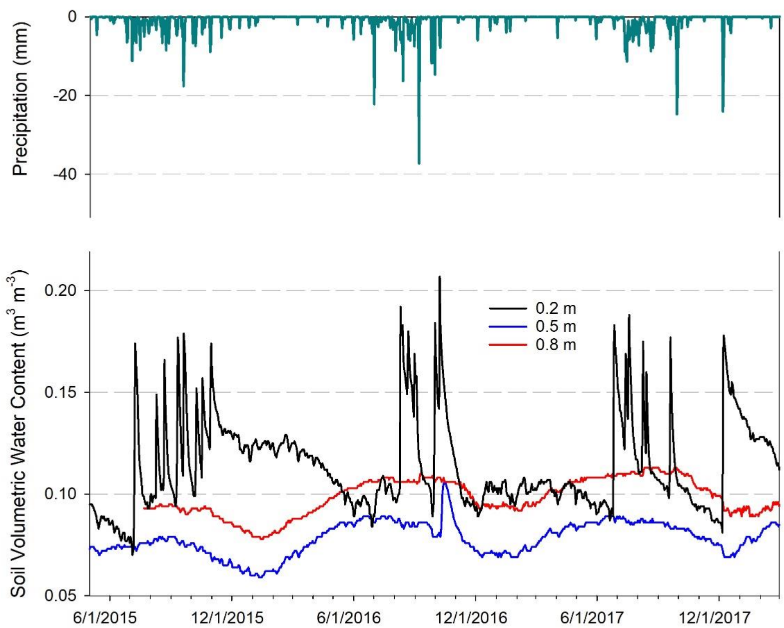

Figure 4. Daily precipitation (P) and soil volumetric water content (θ) levels at 0.2, 0.5, and 0.8 m depths at the North station from 1 May 2015 to 31 March 2017.

The ANOVA results showed no statistical difference ($p > 0.05$) in θ levels between the two sensors installed at 0.2 m and between the two sensors at 0.5 m in each soil water station for either the dry or wet season every year. A significant difference ($p \leq 0.05$) in mean θ levels for dry vs. wet seasons was found for each sensor depth (0.2 and 0.5 m) within each station and between stations. No comparison was performed for the 0.8 m depth.

3.2. Precipitation, Vegetation, and Groundwater Relations

The relationships between monthly *P*, *NDVI*, and *G* values were evaluated from April 2016 to December 2021. Total annual precipitation for the years 2017 (327 mm) and 2022 (390 mm) was greater than the long-term (2007–2022) mean annual precipitation value of 318 mm. The lowest total yearly precipitation value of 124 mm was observed in 2020. The highest monthly total *P* levels that occurred in either July or August were generally followed by the response in vegetation (i.e., *NDVI*) in the following one or two months, then by *G*. The lowest and highest *NDVI* values of 0.16 (June) and 0.37 (August) occurred in 2021. The shallowest *G* levels generally occurred from September to November, except during the driest year (2020), when the shallowest *G* level was observed in January. The values of *G* ranged from 18.9 to 20.2 m, with the deepest *G* value obtained in June 2016 and the shallowest in November 2019 (Table 2).

Table 2. Monthly total of precipitation (*P*, in mm), monthly-average Normalized Difference Vegetation Index (*NDVI*), and monthly-average depth to groundwater (*G*, in m) for years 2016–2021. NA means no data is available.

	2016			2017			2018			2019			2020			2021		
Month	***P***	***NDVI***	***G***	***P***	***NDVI***	***G***	***P***	***NDVI***	***G***	***P***	***NDVI***	***G***	***P***	***NDVI***	***G***	***P***	***NDVI***	***G***
January	4.7	0.19	NA	10.4	0.21	19.3	0.4	0.19	19.1	4.7	0.19	19.1	2.6	0.19	18.9	9.4	0.17	19.7
February	0.6	0.17	NA	1.2	0.19	19.4	3.8	0.19	19.2	3.4	0.18	19.2	5.5	0.18	18.9	10.4	0.18	NA
March	2.3	0.17	NA	0.2	0.17	19.4	1.1	0.18	19.2	4.6	0.17	19.2	19.9	0.19	19.0	0.3	0.17	NA
April	5.1	0.17	20.1	7.4	0.17	19.5	0.7	0.17	19.3	2.7	0.17	19.3	0.2	0.20	19.1	2.1	0.17	NA
May	14.8	0.17	20.2	9.7	0.17	19. 6	3.5	0.18	19.4	3.0	0.17	19.4	1.9	0.19	19.2	1.4	0.17	NA
June	17.2	0.17	20.2	10.8	0.18	19.6	15.1	0.18	19.5	22.7	0.17	19.5	2.7	0.19	19.3	44.0	0.16	NA
July	46.6	0.18	20.2	89.6	0.24	19.7	68.4	0.20	19.5	25.9	0.17	19.6	58.7	0.18	19.6	60.8	0.25	19.7
August	97.0	0.23	20.1	67.7	0.29	19.5	80.8	0.22	19.6	56.2	0.23	19.6	8.2	0.19	19.7	75.5	0.37	19.5
September	93.3	0.32	19.8	73.5	0.23	19.0	45.9	0.31	19.6	91.2	0.27	19.5	12.4	0.18	19.7	44.1	0.33	19.1
October	14.1	0.29	19.3	8.1	0.21	19.1	50.1	0.29	19.4	35.9	0.34	18.9	0.5	0.17	19.7	0.6	0.24	NA
November	4.2	0.23	19.2	1.7	0.19	19.1	0.3	0.25	19.1	31.5	0.25	18.9	0.0	0.17	19.8	5.2	0.21	19.8
December	15.9	0.22	19.2	46.2	0.21	19.1	13.9	0.21	19.1	16.8	0.21	19.0	8.8	0.17	19.8	13.7	0.20	19.3

3.3. Groundwater Levels and Aquifer Recharge

Groundwater levels generally started rising during mid-summer, reaching peak levels in late summer or early fall. The yearly groundwater level rise ranged from 0.7 m in 2018 to 1.3 m in 2022. The exception was during the driest year (2020), when the very low precipitation resulted in groundwater levels declining 1.0 m from the highest level on 10 January to the lowest on 20 November 2020 (Figure 5).

The recharge of the shallow aquifer corresponded to the seasonal rise in the water table built in response to precipitation inputs during the summer and fall every year. When it occurred, yearly *Re* values ranged from 102 to 197 mm, averaging 139 mm. The highest annual *Re* value occurred during the wettest year in 2022. Conversely, no *Re* occurred in 2020 (Table 3).

Table 3. Yearly precipitation (*P*), seasonal changes in groundwater level (Δh), and aquifer recharge (*Re*) for years 2016 to 2022. All data are in mm.

Year	*P*	Δh	*Re*
2016	316	1156	173
2017	327	833	125
2018	289	680	102
2019	299	822	123
2020	122	−997	0
2021	268	761	114
2022	390	1311	197

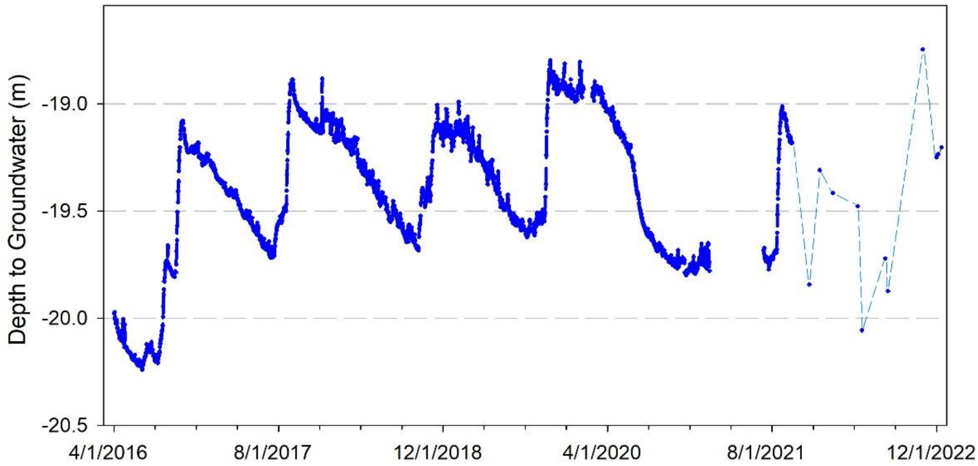

Figure 5. Daily maximum groundwater levels obtained from hourly or bi-hourly records from 1 April 2016 to 16 December 2022. Dashed lines indicate potential groundwater level trajectory connecting manually measured data points in late 2021 and 2022.

3.4. Correlation between Precipitation, Groundwater, Soil Water, and Vegetation Indices

The Spearman Rank Order Correlation test showed a moderate positive correlation ($\rho = 0.314$, $p < 0.01$, $n = 169$) between *G* and *NDVI* and a weak correlation between *G* and *P* ($\rho = 0.108$, $p < 0.01$, $n = 1833$), *P* and *NDVI* ($\rho = 0.272$, $p < 0.01$, $n = 193$), *P* and *NDII* ($\rho = 0.230$, $p < 0.01$, $n = 193$), and θ and *NDVI* ($\rho = 0.168$, $p = 0.03$, $n = 168$). No correlations were found between *G* and θ, *G* and *NDII*, and θ and *NDII*. Figure 6 shows the relationship between *NDVI* and *G*. A threshold of about 20 m depth to groundwater appears to be associated with low *NDVI* values ranging between 0.16 and 0.22.

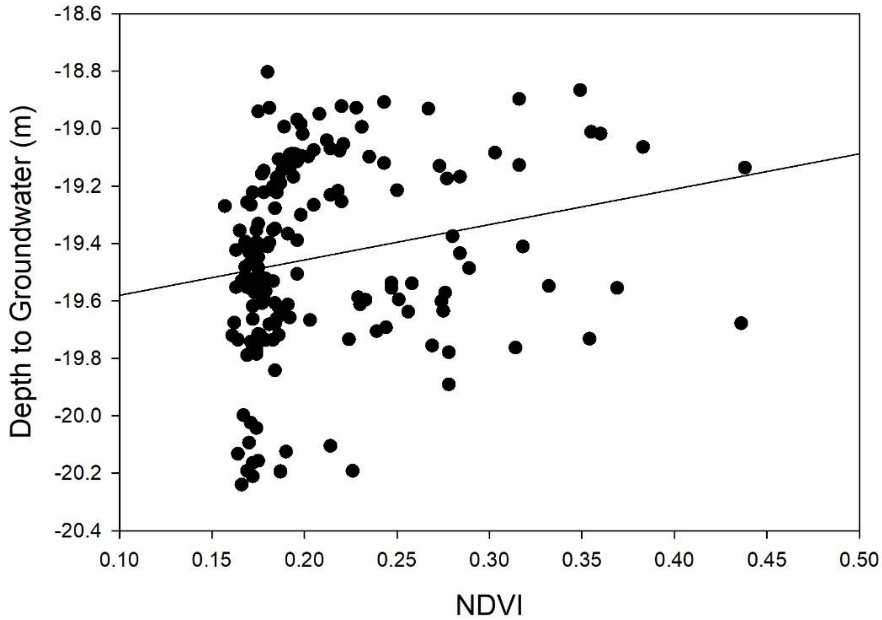

Figure 6. Relationship between depth to groundwater (*G*) and *NDVI*.

3.5. Vegetation Indices—Interannual Variability

Overall, lower *NDVI* values were obtained in the years (2007–2012) before the implementation of the conservation practices for all three zones (Table 4). The exception was in the high elevation zone in 2008, when the maximum *NDVI* value of 0.1919 was greater than the maximum values of 0.1893 and 0.1717 in the post-treatment years 2016 and 2017, respectively.

Table 4. Minimum, mean, and maximum NDVI values from 2007 to 2021.

Z	Stat	2007	2008	2009	2010	2011	2012	2013	2014	2015	2016	2017	2018	2019	2020	2021
Low	Min	0.0693	0.1067	0.0836	0.0740	0.0740	0.0787	0.1564	0.1282	0.1550	0.1348	0.1187	0.1357	0.1085	0.1121	0.1456
	Mean	0.0989	0.1278	0.1004	0.0999	0.0990	0.0991	0.2008	0.1588	0.1824	0.1763	0.1498	0.1604	0.1755	0.1510	0.2051
	Max	0.1481	0.1835	0.1408	0.1395	0.1601	0.1286	0.3189	0.2101	0.2496	0.2300	0.2265	0.2131	0.2700	0.2106	0.3893
Mid	Min	0.0644	0.0940	0.0832	0.0681	0.0654	0.0681	0.1414	0.1246	0.1446	0.1252	0.1175	0.1223	0.1279	0.1114	0.1200
	Mean	0.0990	0.1232	0.0962	0.1011	0.0953	0.1063	0.1908	0.1507	0.1775	0.1566	0.1412	0.1579	0.1657	0.1459	0.2430
	Max	0.1434	0.1655	0.1129	0.1285	0.1261	0.1427	0.2555	0.1939	0.2722	0.2022	0.1878	0.1984	0.2020	0.1860	0.3111
High	Min	0.1088	0.0987	0.0556	0.0915	0.0851	0.0904	0.1539	0.1414	0.1657	0.1311	0.1130	0.1337	0.1392	0.1189	0.2179
	Mean	0.1289	0.1381	0.1034	0.1211	0.1131	0.1305	0.2043	0.1808	0.2066	0.1624	0.1428	0.1702	0.1879	0.1491	0.2898
	Max	0.1600	0.1919	0.1234	0.1690	0.1559	0.1755	0.2459	0.2158	0.2482	0.1893	0.1717	0.2204	0.2297	0.2258	0.3315

Z = Zone.

In the pre-treatment years, *NDVI* values ranged from 0.0693 to 0.1601 in the low elevation zone, from 0.0644 to 0.1655 in the mid-elevation zone, and from 0.0556 to 0.1919 in the high elevation zone. In the post-treatment years (2014–2021), *NDVI* values ranged from 0.1085 to 0.3893 in the low elevation zone, from 0.114 to 0.3111 in the mid-elevation zone, and from 0.1130 to 0.3315 in the high elevation zone (Table 4).

There were significant differences ($p \leq 0.05$) in *NDVI* values by *altitudinal gradient* and by *year*, indicating a difference in the vegetation condition in the low, mid, and high elevation zones and across years. Tukey test results confirmed that the high elevation zone had the highest *NDVI* mean values; this implies that the vegetation condition in this zone is slightly better than that in the mid- and low elevation zones. The Tukey test also confirmed that the years with the lowest and most similar *NDVI* mean values were 2009 to 2012.

Table 5 shows minimum, maximum, and mean *NDII* values from 2007 to 2021. The highest mean annual values for the three elevation zones occurred during the treatment years in 2013. The lowest *NDII* values were obtained for 2020, the driest year. In the pre-treatment years, *NDII* values ranged from −0.1556 to 0.0696 in the low elevation zone, from −0.0913 to 0.0474 in the mid-elevation zone, and from −0.1149 to 0.0658 for the high elevation zone. In the post-treatment years (2014–2021), *NDII* values ranged from −0.1075 to 0.1289 in the low elevation zone, from −0.0828 to 0.0652 in the mid-elevation zone, and from −0.0972 to 0.0617 in the high elevation zone (Table 5).

Table 5. Minimum, mean, and maximum *NDII* values from 2007 to 2021.

Z	Stat	2007	2008	2009	2010	2011	2012	2013	2014	2015	2016	2017	2018	2019	2020	2021
Low	Min	−0.0832	−0.0771	−0.0707	−0.1556	−0.1058	−0.0867	−0.0280	−0.1075	−0.0955	−0.0563	−0.0756	−0.0708	−0.0763	−0.1600	−0.0892
	Mean	−0.0633	−0.0172	−0.0384	−0.0643	−0.0623	−0.0548	0.0189	−0.0427	−0.0419	−0.0045	−0.0372	−0.0111	−0.0298	−0.0836	−0.0442
	Max	−0.0393	0.0696	0.0005	−0.0307	−0.0271	−0.0119	0.1378	0.0190	0.0131	0.0774	0.0836	0.1289	0.0148	−0.0341	0.0056
Mid	Min	−0.0713	−0.0496	−0.0614	−0.0913	−0.0627	−0.1072	−0.0305	−0.0828	−0.0503	−0.0435	−0.0567	−0.0534	−0.0794	−0.1325	−0.0677
	Mean	−0.0379	0.0069	−0.0212	−0.0351	−0.0370	−0.0291	0.0144	−0.0356	−0.0045	−0.0051	−0.0175	0.0088	−0.0072	−0.0401	−0.0135
	Max	0.0113	0.0474	0.0252	0.0195	0.0117	0.0321	0.0709	−0.0033	0.0652	0.0464	0.0460	0.0559	0.0443	0.0163	0.0338
High	Min	−0.0838	−0.0173	−0.1018	−0.0565	−0.1149	−0.0628	−0.0313	−0.0656	−0.0726	−0.0495	−0.0346	−0.0471	−0.0291	−0.1617	−0.0972
	Mean	−0.0189	0.0246	−0.0228	−0.0097	−0.0330	−0.0057	0.0315	−0.0046	0.0077	0.0143	0.0025	0.0073	0.0205	−0.0396	−0.0002
	Max	0.0266	0.0658	0.0293	0.0376	0.0221	0.0425	0.0884	0.0477	0.0476	0.0575	0.0284	0.0617	0.0676	0.0088	0.0434

Z = Zone.

Similar to the *NDVI* results, there were also significant differences ($p \leq 0.05$) in *NDII* values by *altitudinal gradient* and by *year*, which implies a difference in available moisture content in the root zone of the plants at high, mid, and low elevation zones within the study site and over the temporal domain. Tukey test results showed that the highest *NDII* (0.0884) was in the high elevation zone. The lowest *NDII* (−0.1600) value was obtained for the low elevation zone.

3.6. Trend Analysis

The trend analysis showed mixed results for the pre-treatment (2007–2012) and post-treatment years (2014–2021) (Table 6). Sen's slope results indicate that a downward trend for *NDVI* and an upward trend for *T* existed for the pre-treatment period. No trend was detected for *P*. An upward trend for *NDVI* and *T* was noted for the post-treatment years. Similar to pre-treatment years, no trend was seen for *P*. An upward trend for *NDII* was obtained for both pre- and post-treatment periods. The trend analysis based on daily maximum groundwater data available for 2016 to 2022 showed an upward trend in *G* (Table 6).

Table 6. Results from the trend analysis of pre- and post-treatment conditions for the variables evaluated.

Variable	Sen's Slope	*p*-Value
Pre-Treatment (2007–2012)		
Air Temperature	0.00104	<0.001
Precipitation	0.00000	0.240
NDVI	−0.00008	<0.001
NDII	0.00029	<0.001
Post-Treatment (2014–2021)		
Air Temperature	0.00035	<0.001
Precipitation	0.00000	0.840
NDVI	0.00015	<0.001
NDII	0.00035	<0.001
G	0.00013	<0.001

4. Discussion

This research examined the relationships between precipitation, soil water, vegetation, and shallow groundwater in an environmental management unit (EMU) located in a semiarid rangeland ecosystem in the Chihuahuan Desert, northern Mexico.

Similar to other studies that have used remote sensing-based vegetation indices (e.g., [62]) to assess the evolution of the vegetation, the *NDVI* and *NDII* adequately captured plant cover response to the variable interannual precipitation and soil water conditions observed. The conservation practices employed in the EMU have positively affected the state of the rangeland ecosystem. The upward trends in *NDVI*, *NDII*, and *G* observed in the post-treatment years were partly attributed to the improved land conditions. An increased water residence time observed in response to the various conservation methods added, particularly in the higher elevation zone of the study site, appeared to contribute to improved vegetation conditions (Figure A2).

In arid and semiarid regions, vegetation cover is highly correlated with groundwater availability [63]. Similar to our results, Zhu et al. [64] reported that precipitation increased the *NDVI*, leading to a groundwater rise during the wet years in an arid and semiarid region of China. Conversely, the severe drought conditions experienced during the year with the lowest precipitation (2020; 120 mm) were reflected in the deepest *G* (20 m) and lowest *NDVI* (0.17) values obtained for the entire period of study. The positive trend in *G* levels obtained at the study site differs from the drop in groundwater levels reported [45] for most of the regional aquifer in 2010.

NDVI does not account for ground reflectance, making it difficult to interpret when vegetation cover is low (e.g., shrublands) and confused with bare ground [65]. This could have been the case in the *NDVI*, *G*, and *P* monthly relationships analysis when we used *NDVI* values collected during periods of low vegetation cover, typically in the late winter and spring months. To reduce the uncertainty between the reflectance of the soil and the vegetation for the pre- and post-treatment yearly comparisons, we used Landsat imagery captured during the season likely to have the highest amount of biomass at the study site (i.e., August to October). The lack of long-term vegetation data collected on-site makes it challenging to validate the information obtained from the vegetation indices.

While soil properties may differ across the landscape, θ data provides valuable information regarding seasonal precipitation and soil water dynamics critical to vegetation establishment, as well as hydrologic processes such as infiltration and runoff. The overall low θ levels and more muted response in the deeper sensor depths (i.e., 0.5 and 0.8 m depths) observed throughout the study indicate that water transport through the soil profile might have been limited. These results differ from other studies conducted in winter precipitation-dominated rangeland environments, as we have documented relatively rapid soil water transport and deep percolation into the shallow aquifer [25,26].

In summer precipitation-dominated rangeland settings, such as that reported in this study, most of the precipitation that falls during the vegetation growing period in the spring and summer is either lost to direct evaporation or utilized by the vegetation [66]. Several studies show that ephemeral stream losses are an important source of aquifer recharge in arid ecosystems, ranging between 12% and 19% [67,68]. A significant network of ephemeral streams exists throughout the site. Based on the soil water dynamics observed at the study site, it can be inferred that the vertical recharge of the aquifer due to deep percolation in direct response to specific precipitation events at the study site was minimal. Instead, the seasonal replenishment of the local aquifer may have primarily been due to subsurface flow and streambed seepage occurring in the areas of recharge in the upper elevation zone. Under that premise, and based on the available groundwater data, utilizing the WTFM proved a practical and straightforward technique to estimate aquifer recharge.

Some limitations associated with the sole use of the WTFM to estimate groundwater recharge were recognized. Even though the use of the well for livestock and household purposes was minimal, some groundwater level measurements might have been affected, particularly in the latter part of the study when we relied only on a low amount of data collected with the portable water level meter. Given the well's location in the EMU's mid-elevation section, we assumed it was representative of the conditions in the mid- and high elevation zones and captured most of the groundwater recharge from these upper-elevation areas. However, groundwater level fluctuations occurring in the low elevation zone, where a significant amount of the soil and water conservation practices happened, are yet to be fully captured. Groundwater levels can be highly dynamic in a given landscape [63,69]. Future work incorporating the role of vegetation water uptake, soil moisture, and runoff into aquifer recharge estimates could be helpful for comparison with the results obtained by groundwater-based methods, such as the WTFM.

The seasonal groundwater recharge noted during six (out of seven) of the evaluated years was attributed to a combination of factors, including the conservation practices, a relatively shallow aquifer (~20 m), precipitation near or above the long-term mean value, and the location of the monitoring well near the areas of recharge for the local aquifer. However, because of the lack of pre-treatment groundwater level data, no direct causal relationships between the restoration practices and the aquifer recharge estimates obtained in the post-treatment years can be established. Also, the conditions that favored this study's groundwater response to seasonal precipitation in the years following restoration may be absent in other arid or semiarid ecosystems. We might expect a more muted hydrological response with a deeper water table, different geology and location within the regional aquifer, and a drier precipitation regime.

Besides providing critical information to inform the precipitation, soil water, vegetation, and shallow groundwater relationships studied, this research provides an improved understanding of restoration effects on water supply and habitat improvement in desert ecosystems. Surface water and groundwater-dependent terrestrial ecosystems, such as the one found at our study site, include deep- and shallow-rooted vegetation species that are the foundation for the habitat of many mammals, birds, and reptiles. The improved habitat conditions attributed to the conservation practices implemented have increased the number of wildlife species (e.g., javelina, various avian species) observed during the many visits to the study area.

Given the location of our long-term study site in a semiarid area in north-central Chihuahua, this project's findings can inform critical groundwater sustainability issues in the region. The study site is within the Flores Magón-Villa Ahumada regional aquifer which, as reported [45], has experienced significant drops in groundwater levels in recent decades. Results from our study indicate the potential positive effects of rangeland restoration in groundwater replenishment. This raises the question of whether broader restoration efforts can help mitigate the impact of groundwater withdrawals in the region and whether soil and water conservation practices like those utilized in this study can be considered conserved water in a mitigation credit framework, as described in other studies (see for example, [70,71]).

The outcomes of this ongoing long-term study contribute to an improved understanding of the role of conservation practices on ecohydrologic processes in the rangeland ecosystems of northern Mexico. Similar summer precipitation and shallow groundwater conditions can be found throughout the Chihuahuan Desert ecoregion and other dryland environments worldwide. Study findings can contribute to the improved management of rangeland ecosystems through a better understanding of soil, vegetation, and groundwater relations and effective restoration techniques for enhanced habitat and aquifer replenishment. Future research includes the regular collection of field variables, such as runoff and vegetation cover, to strengthen the interpretation of the vegetation and groundwater relationships observed and inform evapotranspiration and groundwater models that can help expand local results to larger spatial and temporal scales.

Author Contributions: C.G.O., C.O.-O., F.V.-G., J.A.P.-A. and H.R.G. developed the study design and conducted field data collection. C.G.O., C.O.-O., F.V.-G., J.A.P.-A., H.R.G. and F.H. contributed to data analysis and the writing of the manuscript. All authors have read and agreed to the published version of the manuscript.

Funding: This research received no external funding.

Institutional Review Board Statement: Not applicable.

Informed Consent Statement: Not applicable.

Data Availability Statement: Most of the data presented in this study are available in the article. Additional information is available upon request.

Acknowledgments: The authors are grateful for the continued support of the Environmental Management Unit (EMU) El Roble. We also want to thank the various graduate and undergraduate students, and faculty, from Universidad Autónoma de Chihuahua who participated in various field data-collection activities related to this research.

Conflicts of Interest: The authors declare no conflict of interest.

Appendix A

Soil and water conservation practices were established in the environmental management unit (EMU) "El Roble" between 2012 and 2014.

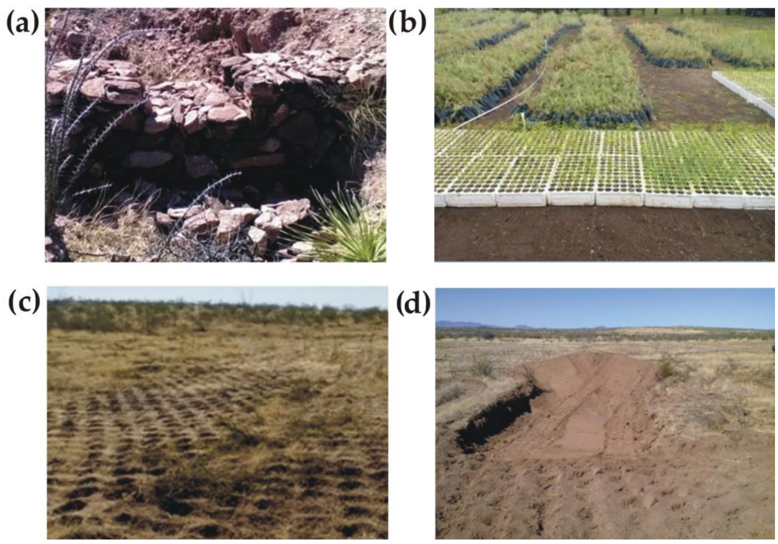

Figure A1. Examples of soil and water conservation practices implemented: (**a**) Gabion, (**b**) Native shrub spp. seedlings (i.e., *Atriplex canescens* and *Prosopis glandulosa*), (**c**) Land imprinting, and (**d**) retention and infiltration pond.

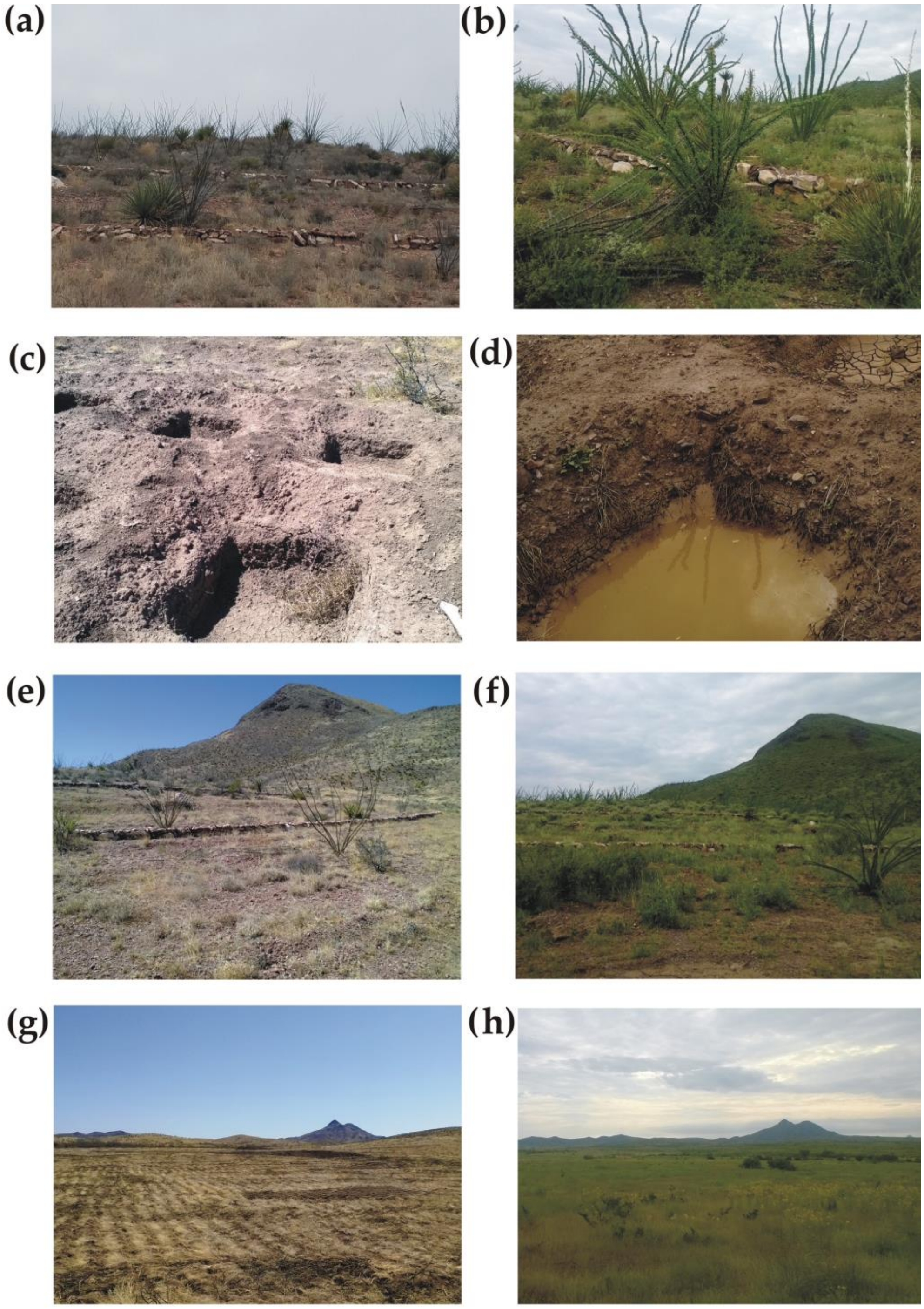

Figure A2. Water and vegetation conditions before and after precipitation for various restoration work, including rock bundles (**a**,**b**), water capture and infiltration pits (**c**,**d**), contour furrows and rock bundles (**e**,**f**), and land imprinting and vegetation response (**g**,**h**).

References

1. Uhlenbrook, S.; Connor, R. *The United Nations World Water Development Report 2019: Leaving No One Behind*; UNESCO: Paris, France, 2019.
2. Schewe, J.; Heinke, J.; Gerten, D.; Haddeland, I.; Arnell, N.W.; Clark, D.B.; Dankers, R.; Eisner, S.; Fekete, B.M.; Colón-González, F.J.; et al. Multimodel assessment of water scarcity under climate change. *Proc. Natl. Acad. Sci. USA* **2014**, *111*, 3245–3250. [CrossRef] [PubMed]

3. Hejazi, M.I.; Edmonds, J.; Clarke, L.; Kyle, P.; Davies, E.; Chaturvedi, V.; Wise, M.; Patel, P.; Eom, J.; Calvin, K. Integrated assessment of global water scarcity over the 21st century under multiple climate change mitigation policies. *Hydrol. Earth Syst. Sci.* **2014**, *18*, 2859–2883. [CrossRef]
4. Pachauri, R.K.; Meyer, L.A. *Climate Change 2014: Synthesis Report. Contribution of Working Groups I, II and III to the Fifth Assessment Report of the Intergovernmental Panel on Climate Change*; IPCC: Geneva, Switzerland, 2014; p. 151.
5. Ojeda Olivares, E.A.; Sandoval Torres, S.; Belmonte Jiménez, S.I.; Campos Enríquez, J.O.; Zignol, F.; Reygadas, Y.; Tiefen-bacher, J.P. Climate Change, Land Use/Land Cover Change, and Population Growth as Drivers of Groundwater Depletion in the Central Valleys, Oaxaca, Mexico. *Remote Sens.* **2019**, *11*, 1290. [CrossRef]
6. Scott, C.; Megdal, S.; Oroz, L.; Callegary, J.; Vandervoet, P. Effects of climate change and population growth on the trans-boundary Santa Cruz aquifer. *Clim. Res.* **2012**, *51*, 159–170.
7. Briggs, M.K.; Lozano-Cavazos, E.A.; Poulos, H.M.; Ochoa-Espinoza, J.J.; Rodriguez-Pineda, J.A. The Chihuahuan Desert: A Binational Conservation Response to Protect a Global Treasure. *Encycl. Worlds Biomes* **2020**, 126–138.
8. Wulder, M.A.; Roy, D.P.; Radeloff, V.C.; Loveland, T.R.; Anderson, M.C.; Johnson, D.M.; Healey, S.; Zhu, Z.; Scambos, T.A.; Pahlevan, N.; et al. Fifty Years of Landsat Science and impacts. *Remote Sens. Environ.* **2022**, *280*, 113195. [CrossRef]
9. Huntington, J.; McGwire, K.; Morton, C.; Snyder, K.; Peterson, S.; Erickson, T.; Niswonger, R.; Carroll, R.; Smith, G.; Allen, R. Assessing the role of climate and resource management on groundwater dependent ecosystem changes in arid environments with the Landsat archive. *Remote Sens. Environ.* **2016**, *185*, 186–197.
10. Aguilar, C.; Zinnert, J.C.; Polo, M.J.; Young, D.R. NDVI as an indicator for changes in water availability to woody vegetation. *Ecol. Indic.* **2012**, *23*, 290–300. [CrossRef]
11. Jia, K.; Liang, S.; Zhang, L.; Wei, X.; Yao, Y.; Xie, X. Forest cover classification using Landsat ETM+ data and time series MODIS NDVI data. *Int. J. Appl. Earth Obs.* **2014**, *33*, 32–38. [CrossRef]
12. Mbatha, N.; Xulu, S. Time series analysis of MODIS-Derived NDVI for the Hluhluwe-Imfolozi Park, South Africa. *Impact of recent intense drought. Climate* **2018**, *6*, 95.
13. Pettorelli, N.; Vik, J.O.; Mysterud, A.; Gaillard, J.M.; Tucker, C.J.; Stenseth, N.C. Using the satellite-derived NDVI to assess ecological responses to environmental change. *Trends Ecol. Evol.* **2005**, *20*, 503–510. [CrossRef] [PubMed]
14. Chuai, X.W.; Huang, X.J.; Wang, W.J.; Bao, G. NDVI, temperature and precipitation changes and their relationships with different vegetation types during 1998–2007 in Inner Mongolia, China. *Int. J. Climatol.* **2013**, *33*, 1696–1706. [CrossRef]
15. Birtwistle, A.N.; Laituri, M.; Bledsoe, B.; Friedman, J.M. Using NDVI to measure precipitation in semi-arid landscapes. *J. Arid Environ.* **2016**, *131*, 15–24. [CrossRef]
16. Wingate, V.R.; Phinn, S.R.; Kuhn, N. Mapping precipitation-corrected NDVI trends across Namibia. *Sci. Total Environ.* **2019**, *684*, 96–112. [CrossRef] [PubMed]
17. Parizi, E.; Hosseini, S.M.; Ataie-Ashtiani, B.; Simmons, C.T. Normalized difference vegetation index as the dominant predicting factor of groundwater recharge in phreatic aquifers: Case studies across Iran. *Sci. Rep.* **2020**, *10*, 17473. [CrossRef]
18. Huang, F.; Ochoa, C.G. A copula incorporated cellular automata module for modeling the spatial distribution of oasis recovered by ecological water diversion: An application to the Qingtu Oasis in Shiyang River Basin, China. *J. Hydrol.* **2022**, *608*, 127573. [CrossRef]
19. Hardisky, M.A.; Klemas, V.; Smart, R.M. The influence of soil salinity, growth form, and leaf moisture on the spectral radiance of Spartina alterniflora canopies. *Photo Eng. Rem. S.* **1983**, *49*, 77–83.
20. Zimba, H.; Coenders-Gerrits, M.; Kawawa, B.; Savenije, H.; Nyambe, I.; Winsemius, H. Variations in canopy cover and its relationship with canopy water and temperature in the miombo woodland based on satellite data. *Hydrology* **2020**, *7*, 58. [CrossRef]
21. Ji, L.; Zhang, L.; Wylie, B.K.; Rover, J. On the terminology of the spectral vegetation index (NIR− SWIR)/(NIR+ SWIR). *Int. J. Remote Sens.* **2011**, *32*, 6901–6909. [CrossRef]
22. Castelli, G.; Oliveira, L.A.A.; Abdelli, F.; Dhaou, H.; Bresci, E.; Ouessar, M. Effect of traditional check dams (jessour) on soil and olive trees water status in Tunisia. *Sci. Total Environ.* **2019**, *690*, 226–236. [CrossRef]
23. Everard, M. Community-based groundwater and ecosystem restoration in semi-arid north Rajasthan (1): Socio-economic progress and lessons for groundwater-dependent areas. *Ecosyst. Serv.* **2015**, *16*, 125–135. [CrossRef]
24. Nemani, R.R.; Keeling, C.D.; Hashimoto, H.; Jolly, W.M.; Piper, S.C.; Tucker, C.J.; Myneni, R.B.; Running, S.W. Climate-driven increases in global terrestrial net primary production from 1982 to 1999. *Science* **2003**, *300*, 1560–1563. [CrossRef] [PubMed]
25. Ochoa, C.G.; Caruso, P.; Ray, G.; Deboodt, T.; Jarvis, W.T.; Guldan, S.J. Ecohydrologic connections in semiarid watershed systems of central Oregon USA. *Water* **2018**, *10*, 181. [CrossRef]
26. Durfee, N.; Ochoa, C.G. The seasonal water balance of juniper-dominated and sagebrush-dominated watersheds. *Hydrology* **2021**, *8*, 156. [CrossRef]
27. Scanlon, B.R.; Healy, R.W.; Cook, P.G. Choosing appropriate techniques for quantifying groundwater recharge. *Hydrogeol. J.* **2002**, *10*, 18–39. [CrossRef]
28. Sophocleous, M. Interactions between groundwater and surface water: The state of the science. *Hydrogeol. J.* **2002**, *10*, 52–67. [CrossRef]
29. Jassas, H.; Merkel, B. Estimating Groundwater Recharge in the Semiarid Al-Khazir Gomal Basin, North Iraq. *Water* **2014**, *6*, 2467–2481. [CrossRef]

30. Risser, D.W.; Gburek, W.J.; Folmar, G.J. Comparison of Recharge Estimates at a Small Watershed in East-Central Pennsylvania, USA. *Hydrogeol. J.* **2009**, *17*, 287–298. [CrossRef]
31. Varni, M.; Comas, R.; Weinzettel, P.; Dietrich, S. Application of the water table fluctuation method to characterize groundwater recharge in the Pampa plain, Argentina. *Hydrolog. Sci. J.* **2013**, *58*, 1445–1455. [CrossRef]
32. Healy, R.W.; Cook, P.G. Using Groundwater Levels to Estimate Recharge. *Hydrogeol. J.* **2002**, *10*, 91–109. [CrossRef]
33. Childs, E.C. The nonsteady state of the water table in drained land. *J. Geophys. Res.* **1960**, *65*, 780–782. [CrossRef]
34. Siyag, P.R. Site Selection, Survey and Treatment Plan. In *Afforestation, Reforestation and Forest Restoration in Arid and Semi-Arid Tropics*; Siyag, P.R., Ed.; Springer: Dordrecht, The Netherlands; Bonn, Germany, 2014; pp. 51–78.
35. Gebrernichael, D.; Nyssen, J.; Poesen, J.; Deckers, J.; Haile, M.; Govers, G.; Moeyersons, J. Effectiveness of stone bunds in controlling soil erosion on cropland in the Tigray Highlands, northern Ethiopia. *Soil Use Manage.* **2005**, *21*, 287–297. [CrossRef]
36. Ponce-Rodríguez, M.D.C.; Prieto-Ruíz, J.Á.; Carrete-Carreón, F.O.; Pérez-López, M.E.; Muñoz-Ramos, J.D.J.; Reyes-Estrada, O.; Ramírez-Garduño, H. Influence of stone bunds on vegetation and soil in an area reforested with Pinus engelmannii Carr. in the forests of Durango, Mexico. *Sustainability* **2019**, *11*, 5033. [CrossRef]
37. Negusse, T.; Yazew, E.; Tadesse, N. Quantification of the impact of integrated soil and water conservation measures on groundwater availability in Mendae Catchment, Abraha We-Atsebaha, eastern Tigray, Ethiopia. *Momona Ethiop. J. Sci.* **2013**, *5*, 117–136. [CrossRef]
38. García-Ávalos, S.; Rodriguez-Caballero, E.; Miralles, I.; Luna, L.; Domene, M.A.; Solé-Benet, A.; Cantón, Y. Water harvesting techniques based on terrain modification enhance vegetation survival in dryland restoration. *Catena* **2018**, *167*, 319–326. [CrossRef]
39. Radonic, L. Re-conceptualising water conservation: Rainwater harvesting in the desert of the southwestern United States. *Water Altern.* **2019**, *12*, 699–714.
40. Jahantigh, M.; Pessarakli, M. Utilization of contour furrow and pitting techniques on desert rangelands: Evaluation of runoff, sediment, soil water content and vegetation cover. *J. Food Agric. Environ* **2009**, *7*, 736–739.
41. Schmidt, R.H., Jr. A climatic delineation of the 'real' Chihuahuan Desert. *J. Arid Environ.* **1979**, *2*, 243–250. [CrossRef]
42. Pool, D.B.; Panjabi, A.O.; Macias-Duarte, A.; Solhjem, D.M. Rapid expansion of croplands in Chihuahua, Mexico threatens declining North American grassland bird species. *Biol. Conserv.* **2014**, *170*, 274–281. [CrossRef]
43. Instituto Nacional de Geografía e Infotmatica (INEGI). Edafología. Available online: https://www.inegi.org.mx/temas/edafologia/#Descargas (accessed on 12 October 2022).
44. Sistema Nacional de Información del Agua (SINA). Regiones Hidrológicas (Nacional). Available online: https://sina.conagua.gob.mx/sina/tema.php?tema=regionesHidrologicas (accessed on 12 October 2022).
45. Comisión Nacional del Agua (CONAGUA). *Actualización de la Disponibilidad Media Anual de Agua en el Acuífero Flores Magón-Villa Ahumada (0821)*; Estado de Chihuahua; Subdirección General Técnica Gerencia de Aguas Subterráneas: Ciudad De México, México, 2020; p. 27.
46. Huang, S.; Tang, L.; Hupy, J.P.; Wang, Y.; Shao, G. A commentary review on the use of normalized difference vegetation index (NDVI) in the era of popular remote sensing. *J. Forestry Res.* **2021**, *32*, 1–6. [CrossRef]
47. Zhang, S.; Ye, Z.; Chen, Y.; Xu, Y. Vegetation responses to an ecological water conveyance project in the lower reaches of the Heihe River basin. *Ecohydrology* **2017**, *10*, e1866. [CrossRef]
48. Chen, X.; Vierling, L.; Deering, D.; Conley, A. Monitoring boreal forest leaf area index across a Siberian burn chronosequence: A MODIS validation study. *Int. J. Remote Sens.* **2005**, *26*, 5433–5451. [CrossRef]
49. Verbesselt, J.; Hyndman, R.; Zeileis, A.; Culvenor, D. Phenological change detection while accounting for abrupt and gradual trends in satellite image time series. *Remote Sens. Environ.* **2010**, *114*, 2970–2980. [CrossRef]
50. Jordan, C.F. Derivation of leaf-area index from quality of light on the forest floor. *Ecology* **1969**, *50*, 663–666. [CrossRef]
51. Rouse, J.W.; Haas, R.H.; Deering, D.W.; Schell, J.A.; Harlan, J.C. *Monitoring the Vernal Advancement and Retrogradation (Green Wave Effect) of Natural Vegetation*; Texas A&M University: Austin, TX, USA, 1974; pp. 1–8.
52. Friesen, J.; Steele-Dunne, S.C.; van de Giesen, N. Diurnal differences in global ERS scatterometer backscatter observations of the land surface. *IEEE T. Geosci. Remote.* **2012**, *50*, 2595–2602. [CrossRef]
53. van Emmerik, T.; Steele-Dunne, S.C.; Judge, J.; van de Giesen, N. Impact of diurnal variation in vegetation water content on radar backscatter from maize during water stress IEEE T. *Geosci. Remote.* **2015**, *53*, 3855–3869. [CrossRef]
54. Sriwongsitanon, N.; Gao, H.; Savenije, H.H.; Maekan, E.; Saengsawang, S.; Thianpopirug, S. Comparing the Normalized Difference Infrared Index (NDII) with root zone storage in a lumped conceptual model. *Hydrol. Earth Syst. Sc.* **2016**, *20*, 3361–3377. [CrossRef]
55. Loveland, T.R.; Dwyer, J.L. Landsat: Building a strong future. *Remote Sens. Environ.* **2012**, *122*, 22–29. [CrossRef]
56. Wulder, M.A.; Loveland, T.R.; Roy, D.P.; Crawford, C.J.; Masek, J.G.; Woodcock, C.E.; Allen, R.G.; Anderson, M.C.; Belward, A.S.; Cohen, W.B.; et al. Current status of Landsat program, science, and applications. *Remote Sens. Environ.* **2019**, *225*, 127–147. [CrossRef]
57. Banskota, A.; Kayastha, N.; Falkowski, M.J.; Wulder, M.A.; Froese, R.E.; White, J.C. Forest monitoring using Landsat time series data: A review. *Can. J. Remote Sens.* **2014**, *40*, 362–384. [CrossRef]
58. Gorelick, N.; Hancher, M.; Dixon, M.; Ilyushchenko, S.; Thau, D.; Moore, R. Google Earth Engine: Planetary-scale geospatial analysis for everyone. *Remote Sens. Environ.* **2017**, *202*, 18–27. [CrossRef]

59. Ni, J. Estimating net primary productivity of grasslands from field biomass measurements in temperate northern China. *Plant Ecol.* **2004**, *174*, 217–234. [CrossRef]
60. Fajardo, J.; Lessmann, J.; Bonaccorso, E.; Devenish, C.; Munoz, J. Combined use of systematic conservation planning, species distribution modelling, and connectivity analysis reveals severe conservation gaps in a megadiverse country (Peru). *PloS ONE* **2014**, *9*, e114367. [CrossRef] [PubMed]
61. Realyvazquez-Valencia, M.T. Variables Relacionadas Con La Dinámica Del Nivel De Agua En El Subsuelo De Una Microcuenca Del Desierto Chihuahuense. Master's Thesis, Universidad Autónoma de Chihuahua, Chihuahua, Mexico, 2021.
62. Huang, F.; Ochoa, C.G.; Chen, X.i.; Cheng, Q.; Zhang, D. An entropy-based investigation into the impact of ecological water diversion on land cover complexity of restored oasis in arid inland river basins. *Ecol. Eng.* **2020**, *151*, 105865. [CrossRef]
63. Huang, F.; Zhang, Y.; Zhang, D.; Chen, X. Environmental Groundwater Depth for Groundwater-Dependent Terrestrial Ecosystems in Arid/Semiarid Regions: A Review. *Int. J. Environ. Res. Public Health* **2019**, *16*, 763. [CrossRef]
64. Zhu, L.; Gong, H.; Dai, Z.; Xu, T.; Su, X. An integrated assessment of the impact of precipitation and groundwater on vegetation growth in arid and semiarid areas. *Environ. Earth Sci.* **2015**, *74*, 5009–5021. [CrossRef]
65. Montandon, L.; Small, E. The impact of soil reflectance on the quantification of the green vegetation fraction from NDVI. *Remote Sens. Environ.* **2008**, *112*, 1835–1845. [CrossRef]
66. Wilcox, B.P.; Seyfried, M.S.; Breshears, D. *Encyclopedia of Water Science*; Marcel Dekker, Inc.: New York, NY, USA, 2003; pp. 791–794.
67. Stonestrom, D.A.; Constantz, J.; Ferre, T.P.A.; Stanley, S.A. *Ground-Water Recharge in the Arid and Semiarid Southwestern United States*; U.S. Geological Survey Professional Paper 1703: Reston, VA, USA, 2007; p. 414.
68. Coes, A.L.; Pool, D.R. Ephemeral-stream channel and basin-floor infiltration and recharge in the Sierra Vista subwatershed of the Upper San Pedro Basin, southeastern Arizona. In *Ground-Water Recharge in the Arid and Semiarid Southwestern United States*; Stonestrom, D.A., Constantz, J., Ferre, T.P.A., Stanley, S.A., Eds.; U.S. Geological Survey Professional Paper 1703: Reston, VA, USA, 2007; pp. 253–311.
69. Taylor, C.J.; Alley, W.M. *Ground-Water-Level Monitoring and the Importance of Long-Term Water-Level Data*; US Geological Survey Circular 1217: Denver, CO, USA, 2001; pp. 1–63.
70. Grimm, M. Metrics and Equivalence in Conservation Banking. *Land* **2021**, *10*, 565. [CrossRef]
71. McKenney, B.A.; Kiesecker, J.M. Policy development for biodiversity offsets: A review of offset frameworks. *Env. Manage.* **2010**, *451*, 65–76. [CrossRef]